Proof of CMB-driven X-ray brightening of high-z radio galaxies

Edmund Hodges-Kluck[1], Elena Gallo[2], Gabriele Ghisellini[3], Francesco Haardt[4,5], Jianfeng Wu[6], Benedetta Ciardi[7]

[1] *NASA/GSFC, Code 662, Greenbelt, MD 20771, USA*

[2] *Department of Astronomy, University of Michigan, 1085 S University Ave, Ann Arbor, MI 48109, USA*

[3] *INAF – Osservatorio Astronomico di Brera, Via Bianchi 46, I-23807 Merate, Italy*

[4] *Universitá degli Studi dell'Insubria, Via Valleggio 11, I-22100 Como, Italy*

[5] *INFN, Sezione Milano-Bicocca, P.za della Scienza 3, I-20126 Milano, Italy*

[6] *Department of Astronomy, Xiamen University, Xiamen, Fujian 361005, China*

[7] *Max Planck Institute for Astrophysics, Karl-Schwarzschild-Strasse 1, D-85748 Garching bei München, Germany*

6 May 2021

ABSTRACT

We present a definitive assessment of the role of Inverse Compton scattering of Cosmic Microwave Background photons (IC/CMB) in the context of radio galaxies. Owing to the steep increase of the CMB radiation energy density, IC/CMB is supposed to become progressively more important with respect to radio synchrotron cooling as the redshift increases. For typical energies at play, this process will up-scatter the CMB photons into the X-ray band, and is thus expected to yield a redshift-dependent, concurrent X-ray brightening and radio dimming of the jet-powered structures. Here we show how a conclusive proof of this effect hinges on high-resolution imaging data in which the extended lobes can be distinguished from the compact hot spots where synchrotron-self-Compton dominates the X-ray emission regardless of redshift. We analyze Chandra and Very Large Array data of 11 radio galaxies between $1.3 \lesssim z \lesssim 4.3$, and demonstrate that the emission from their lobes is fully consistent with the expectations from IC/CMB in equipartition. Once the dependence on size and radio luminosity are properly accounted for, the measured lobe X-ray luminosities bear the characteristic $\propto (1 + z)^4$ proportionality expected of a CMB seed radiation field. Whereas this effect can effectively quench the (rest-frame) GHz radio emission from $z \gtrsim 3$ radio galaxies below $\lesssim 1$ mJy, IC/CMB alone can not be responsible for a deficit in high-z, radio-loud AGN if–as we argue–such AGN typically have bright, compact hot spots.

Key words: galaxies: active — galaxies: high-redshift — galaxies: jets — radiation mechanisms: non–thermal — X-rays: galaxies

1 INTRODUCTION

Radio emission from active galactic nuclei (AGN) is typically associated with magnetized jets of relativistic, charged particles launched very close to the central engine that produce synchrotron emission. These jets are important not just to understanding the AGN phenomenon, but also as agents of AGN "feedback" in galaxies (e.g., Moster et al. 2010) and galaxy clusters (Fabian 2012), where AGN energy is needed to (re-)heat or expel gas to prevent much more rapid star formation than is observed. In a minority of AGN– including radio galaxies, radio-loud quasars and blazars–the radio luminosity substantially exceeds the optical luminosity; these are usually referred to as radio-loud AGN. Although the most radio-

luminous AGN are canonically associated with very massive black holes, core radio emission from compact jets appears ubiquitous across the black hole mass function, including in low-luminosity AGN (Nagar et al. 2005) and dwarf galaxies (Reines et al. 2020). By analogy with Galactic black-hole X-ray binaries, the presence (and to some extent the luminosity) of a collimated jet depends strongly on the ratio of the mass accretion rate to the Eddington limit (Fender et al. 2004). Thus, the frequency of radio-loud AGN as a function of redshift could be sensitive to the formation mechanism and evolution of massive black holes over cosmic time, as well as their impact on the galaxies or clusters that occupy the same dark matter halo.

Below $z \lesssim 2$, the fraction of radio-loud quasars is 10-20% (Kellermann et al. 1989; Padovani 1993). There is some evidence

that the radio-loud fraction evolves with redshift (e.g., Jiang et al. 2007), but this remains a matter of debate (e.g., Bañados et al. 2015). One confounding effect is that the expected observability of even the brightest, intrinsically radio-loud AGN at higher redshifts is questionable (Ajello et al. 2009; Volonteri et al. 2011; Ghisellini et al. 2014). This is because the relativistic particles that emit radio synchrotron emission can also cool via Inverse Compton (IC) scattering, in which an ambient or external photon field is boosted by interaction with higher-energy particles and leaves the system. Since the energy density of the CMB radiation scales as $u_{\rm CMB} \propto (1+z)^4$, cooling from IC scattering of the Cosmic Microwave Background photons (hereafter IC/CMB) is expected to become increasingly important at progressively higher redshifts, and eventually overtake synchrotron cooling. IC scattering boosts photons of initial frequency ν_0 to $\nu_1 \approx 4\nu_0\gamma^2/3$, where γ is the relativistic particle Lorentz factor. Since $\nu_{\rm CMB} = 160.4(1+z)$ GHz, CMB photons will be scattered in the X-ray band for $\gamma \gtrsim 700(1+z)^{-1/2}$. Under the usual assumption that the jet particle energies are distributed as a power law with $N(\gamma) \propto \gamma^{-p}$, and with typical bounds of $10 < \gamma < 10^4$ (Worrall & Birkinshaw 2006), then a significant fraction of the total IC/CMB luminosity will land in the (rest-frame) X-ray band. Thus, in the context of jetted AGN, IC/CMB is expected to produce X-rays from the same regions where the radio synchrotron emission is usually observed.

This mechanism will compete with synchrotron cooling in such a way that the ratio of the IC/CMB to synchrotron luminosity–which is well approximated by the $L_{\rm X}/L_{\rm r}$ ratio–is equal to the ratio of the CMB to local magnetic energy density, $u_{\rm CMB}/u_{\rm B}$. Assuming that radio-loud AGN have a somewhat well-defined, redshift independent, average $u_{\rm B}$, then one expects that the ratio $L_{\rm X}/L_{\rm r}$ increases as $(1+z)^4$. This implies a concurrent, redshift-dependent X-ray brightening and radio dimming of jetted AGN, so much so that these objects could possibly be disguised as radio-quiet AGN in spite of having powerful jets. This process is often referred to as CMB quenching (Ghisellini et al. 2015a).

Although this expectation is marginally supported by the discovery of jets that are *only* visible in the X-rays (Simionescu et al. 2016; Schwartz et al. 2020), so far there is no compelling evidence that, for radio-loud AGN, $L_{\rm X}/L_{\rm r}$ is strongly correlated with redshift. Smail et al. (2012) and Smail & Blundell (2013) measured $L_{\rm X}/L_{\rm r}$ in a sample of high-z radio galaxies[1] with the Chandra X-ray Observatory and interferometric radio data, and found no correlation with redshift. Instead, Smail & Blundell (2013) noticed a weak correlation between $L_{\rm X}/L_{\rm r}$ and the far-infrared luminosity, which led them to posit that IC scattering of local far-infrared photons (IC/FIR) dominates the IC X-ray emission instead. Likewise, fitting the spectral energy distributions of a few high-z radio galaxies with a multi-component jet model, Wu et al. (2017) found evidence for X-ray IC/CMB emission consistent with a redshift enhancement in a few high-z systems, but left open the possibility that many IC seed photons are FIR photons from the host. Meanwhile, Zhu et al. (2019) measured enhanced X-ray emission in highly radio-loud quasars at $z > 4$, using a two-point spectral index analysis, but they concluded that the enhancement is too weak to be explained by a dominant role for IC/CMB at all redshifts (see also Miller et al. 2011; Wu

et al. 2013). Ighina et al. (2019) found that the average $L_{\rm X}/L_{\rm r}$ of radio-selected blazars at $z > 4$ is higher than those at lower redshift, but without a strong correlation. Similar to Zhu et al. (2019), they interpreted the enhancement as due to increased, but not dominant, IC/CMB.

In summary, whereas IC scattering of CMB photons off of relativistic AGN jet particles ought to (i) take place, so long as the CMB exists, and (ii) increase in relative strength with redshift, observational evidence for this effect is thin at best. In this paper, we demonstrate how the most likely explanation for this tension does not hinge on the presence of an additional seed photon field for IC. Rather, we show how prior studies have measured or inferred the $L_{\rm X}/L_{\rm r}$ ratio from the integrated emission of the lobes plus the hot spots (and, occasionally, the core and jets as well). This, we argue, effectively washes out any possible redshift dependence, even for sources with similar lobe sizes.

Throughout this work we adopt the following cosmology: $H_0 = 69.6$ km s^{-1} Mpc^{-1}, $\Omega_{\rm M} = 0.286$, and $\Omega_{\rm vac} = 0.714$ (Bennett et al. 2014).

2   INVERSE COMPTON SCATTERING OF CMB PHOTONS IN EQUIPARTITION

The lobes of powerful low-z radio galaxies are typically close to equipartition between the magnetic field and relativistic particle energy density with $B \sim 0.3 - 1.3B_{\rm eq}$ and a strong peak near $0.7B_{\rm eq}$ (Croston et al. 2005; Kataoka & Stawarz 2005). In equipartition, $u_{\rm B} = B_{\rm eq}^2/8\pi$ can be estimated from the measured synchrotron luminosity, $L_{\rm sync}$, and emitting volume V as:

$$B_{\rm eq} = \left[6\pi(1+k)c_{12}L_{\rm sync}\phi^{-1}V^{-1}\right]^{2/7},\tag{1}$$

where k is the ratio of energy in protons to electrons, the function c_{12} depends on the frequency range and spectral index (Pacholczyk 1970), and ϕ is the lobes' filling factor; the bulk of the synchrotron radiation is emitted in the radio band. Since we know how $u_{\rm CMB}$ evolves, we can then predict the luminosity arising from IC/CMB (as noted in § 1, the Comptonized CMB photons will be boosted to X-ray energies for the typical parameters at play in radio galaxies). Notice that this is a lower bound to the actual expected luminosity because synchrotron self-Compton (SSC) could also produce X-rays. If IC/CMB is the only X-ray source, then the ratio of the X-ray luminosity expected from IC/CMB to the measured radio synchrotron luminosity can be written as:

$$\frac{L_{\rm IC/CMB}}{L_{\rm sync}} = \frac{u_{\rm CMB}}{u_{\rm B}} \simeq \frac{L_{\rm X,CMB}}{L_{\rm r}} = \frac{8\pi a T_0^4 (1+z)^4}{B^2},\tag{2}$$

where $a = 7.5658 \times 10^{-15}$ erg cm^{-3} K^{-4} is the radiation constant and $T_0 = 2.725$ K is the temperature of the CMB at $z = 0$. If we assume a spherical volume $(4/3)\pi r^3$, then equipartition implies that

$$L_{\rm X,CMB} = L_{\rm r}^{3/7}\left[\frac{8\pi a T_0^4 (1+z)^4}{(\frac{9}{2}(1+k)c_{12})^{4/7}}(r^3\phi)^{4/7}\right].\tag{3}$$

We adopt $\phi = 1$, $k = 0$ (electrons and positrons only), and $c_{12} = 5 \times 10^7$. Assuming that the spectral index $\alpha \approx 0.7$ from 10 MHz

---

[1] Radio-loud AGN whose radio emission is resolved into separate components, possibly including a core, jet, "hot spots," and diffuse lobes

up to 1-10 GHz, then $3 < c_{12}/10^7 < 10$. The X-ray band tends to probe electrons not yet affected by spectral ageing. This leads to:

$$\left(\frac{L_{\mathrm{X,CMB}}}{10^{45}\ \mathrm{erg\ s^{-1}}}\right) = 2.6 \times 10^{-5} \left(\frac{L_{\mathrm{r}}}{10^{45}\ \mathrm{erg\ s^{-1}}}\right)^{3/7} r_{\mathrm{kpc}}^{12/7}(1+z)^4, \quad (4)$$

where r_{kpc} is the emitting region radius expressed in units of kpc. If we can measure the size of the emitting region, and its radio luminosity, we can predict the IC/CMB X-ray luminosity in equipartition. We can then compare the predicted and measured X-ray luminosities to determine whether these assumptions are sufficient to explain the observations. Throughout this paper, we use rest-frame luminosities.

Here we perform this measurement for a small sample of high-z radio galaxies with archival Chandra X-ray Telescope data. With its sub-arcsecond resolution, Chandra is necessary to resolve the X-ray emission from the lobes (vs. the hot spots), and to more closely match the resolution of the interferometric radio data. It is crucial to make this comparison in the lobes and hot spots *separately*; albeit both may be in equipartition, Equation 4 predicts a very different $L_{\mathrm{X}}/L_{\mathrm{r}}$ ratio in the large, weakly magnetized lobes (higher $L_{\mathrm{X}}/L_{\mathrm{r}}$) as opposed to the small, strongly magnetized hot spots (lower $L_{\mathrm{X}}/L_{\mathrm{r}}$). In addition, SSC is likely to play a dominant role in the hot spots (Section 4), enhancing their X-ray luminosity independent of redshift, so a clean and definitive test of whether the extended emission from radio galaxies is consistent with the expectations from IC/CMB in equipartition is to be carried out in the lobes.

3 RADIO AND X-RAY LUMINOSITY MEASUREMENTS

3.1 High-redshift radio galaxy sample

The working sample includes 11 high-z radio galaxies observed with Chandra (an additional system, TN J0924−2201, has a proprietary Chandra observation). We loosely define a high-z radio galaxy as a radio galaxy at $z > 1$, and the goal is not to have a complete sample of high-z radio galaxies (which does not exist in the Chandra archive), but rather to test whether the lobes are in equipartition, and thus brighten as $(1+z)^4$ due to IC/CMB. As such, the sample is biased towards high-z radio galaxies luminous enough to be observed by Chandra, and we further reject systems where the X-ray emission cannot be reliably decomposed into a core and extended components, the system is embedded in a bright intra-cluster medium (at $z \lesssim 2$), or where the extended emission is only a jet. In these latter systems, it is likely that much or all of the X-ray emission is synchrotron emission from a very energetic population of cosmic rays (Meyer et al. 2015; Georganopoulos et al. 2016), which confounds the comparison we want to make (however, see Worrall et al. 2020, for examples of IC/CMB jet emission). Examples of rejected high-z radio galaxies include 3C 294 ($z = 1.779$), which is surrounded by bright thermal emission, and 3C 191 ($z = 1.956$), whose diffuse radio emission occurs in a region severely contaminated by the image of the core (i.e., the point-spread function wings).

Despite these limitations, the sample is sufficient to ask whether high-z radio galaxies are similar to more local analogs and to estimate how close they are to equipartition. The high-z radio galaxies in the sample, along with the radio and X-ray data we used, are listed in Table 1. Radio and X-ray images with the relevant regions labeled are shown in Figure 1, and the measurements are presented in Tables 2, 3, and 4.

3.2 Radio Data

We measured radio fluxes from Karl G. Jansky Very Large Array (VLA) images with resolution of about an arcsecond. The available data span a range of frequencies (1.4–25 GHz) and quality, and often there are no images from compact arrays or single-dish telescopes that allow us to measure the total flux. Hence, some of the diffuse lobe emission may be resolved out. We retrieved pipeline-processed images from the VLA data archive where they exist, and followed the standard pipeline using the CASAPY software (McMullin et al. 2007) to create CLEANed images in the other cases, using the bandpass and gain calibrators appropriate for each observation. The data sets used are listed in Table 1.

We measured fluxes from lobes and hot spots as described below, and report rest-frame luminosities as:

$$L_{\nu,\mathrm{rest}} = 4\pi d_{\mathrm{L}}^2 (1+z)^{\alpha-1}(\nu_{\mathrm{rest}}/\nu_{\mathrm{obs}})^{-\alpha} F_\nu \quad (5)$$

where α is defined so that $F_\nu \propto \nu^{-\alpha}$ and is measured in the GHz band. We report luminosities as νL_ν. Note that for $\alpha = 1$, the redshift dependence cancels out. High-z radio galaxies are sometimes ultra-steep-spectrum sources, so α may be larger in the observed-frame GHz band than for the electrons most relevant to IC/CMB. However, at low frequencies the angular resolution is worse and decomposing the system into lobes and hot spots is not generally possible, so we cannot directly test this possibility in each component.

3.3 X-ray Data

We measured X-ray fluxes from Chandra Advanced CCD Imaging Spectrometer (ACIS) images. We retrieved the data from the archive and processed it into analysis-ready level=2 files using the Chandra Interactive Analysis of Observations (CIAO v4.12; Fruscione et al. 2006) software. This involved using the CIAO *chandra_repro* script to reduce and calibrate the data, merging data sets for the same target where appropriate (i.e., same detector, exposure time, etc.), restricting the energy range from 0.5–8.0 keV to maximize the signal, and astrometrically registering the X-ray data against the radio images or optical catalogs. We then used the same regions defined before to measure X-ray count rates, from which we subtracted a mean on-field background. In the case of non-detection, the upper limit was measured using the expected number of background counts as the mean of a Poisson distribution, then determining the number of counts at which there is a 99.73% likelihood that a counts cluster is a real source.

To convert the count rate to X-ray luminosities, we use the appropriate Chandra response for each epoch, account for pile-up where necessary, subtract a local background, and assume that all the emission is IC/CMB with a spectral index of $\alpha = 1$ ($\Gamma = 2$). We further assume that there is only absorption from the Galactic column density (computed from the HI4PI survey; HI4PI Collaboration et al. 2016), and that a rest-frame 2–10 keV luminosity is appropriate for comparison to the radio data. In some high-z radio galaxies at $z \lesssim 2$ there is known to be X-ray emission from intra-cluster plasma. It is also possible that a source embedded in a denser medium will be surrounded by a cocoon of shock-heated gas. However, the signal is insufficient to extract a high fidelity spectrum, and in the cases where we can extract a spectrum it is consistent with a power law.
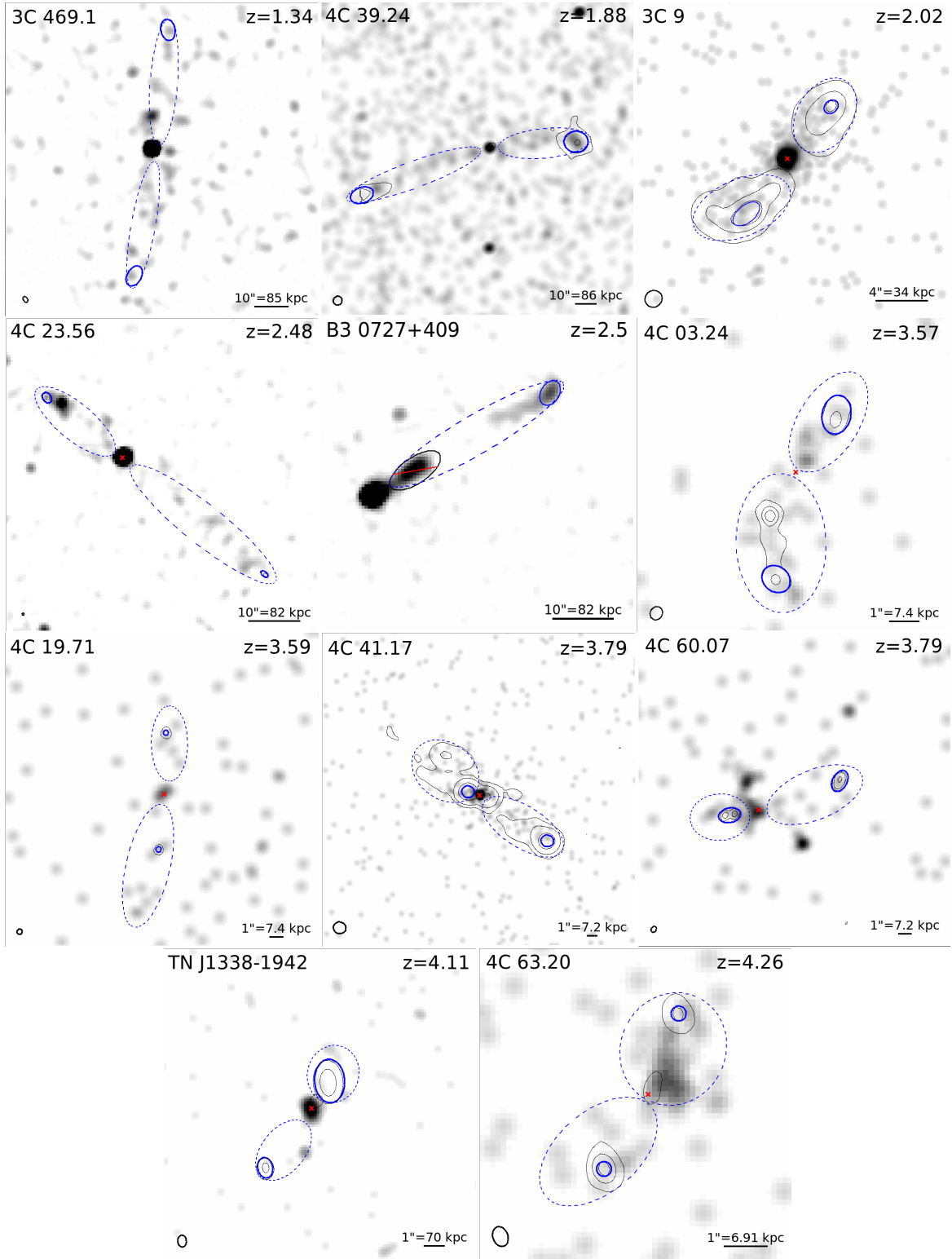
Figure 1. Images of 11 high-z radio galaxies with public Chandra data. The grey scale image is the 0.5-8 keV Chandra image, smoothed with a Gaussian kernel to enhance low intensity emission. Radio contours are overlaid in black (the radio beam is depicted as a black ellipse in the left corner of each image), while the lobe and hot spot regions used in the text are shown as blue dashed and thick ellipses, respectively. We excise the core emission, and assume the total "lobe" volume when computing the total lobe+hot spot emission (see text). Radio contours are listed in units of mJy per beam: 3C 469.1 (3, 18), 4C +39.24 (1, 10), 3c 9 (4, 50, 200), 4C +23.56 (0.8, 3), B3 0727+409 (<2, non-detection), 4C +03.24 (1, 5, 10), 4C +19.71 (4, 20), 4C +41.17 (0.5, 1, 25), 4C +60.07 (0.4, 0.8, 10), TN J1338−1942 (1, 10), and 4C +63.20 (1, 5, 25).

Table 1. Radio galaxies examined in this work.

Name	R.A. (J2000)	Dec. (J2000)	z	VLA Program	Date	Freq. (GHz)	Chandra ObsID	Date	Sum GTI (ks)
3C 469.1	23:55:23.32	+79:55:19.6	1.336	AR0125	1985-02-21	1.49	9260	2009-05-24	20.2
				AR0125	1985-06-01	4.89			
4C +39.24	09:08:16.919	+39:43:26.3	1.883	AB1093	2004-09-18	1.45	5265	2005-03-02	19.9
				AA0150	1993-04-18	1.45			
3C 9	00:20:25.219	+15:40:54.59	2.02	AL280	1992-12-13	1.55	1595	2001-06-10	82.6
							17088	2015-11-02	
							18700	2015-11-03	
							18701	2015-11-04	
4C +23.56	21:07:14.82	+23:31:45	2.483	AC0374	1994-03-18	4.74	11687	2009-08-16	92.9
				AR409	1999-05-28	4.84			
B3 0727+409	07:30:51.346	+40:49:50.8	2.5	PERL2	1995-07-24	1.45	18184	2016-12-12	132.2
							19959	2016-12-12	
							19960	2016-12-14	
4C +03.24	12:45:38.364	+03:23:20.7	3.57	AM0336	1991-08-20	1.51	12288	2010-05-10	92.0
				AC0374	1994-03-18	4.74			
4C +19.71	21:44:07.481	+19:29:15.4	3.59	AC0374	1994-03-18	4.74	12287	2010-08-23	91.7
				AC0374	1994-03-18	8.24	13024	2010-08-26	
4c +41.17	06:50:52.098	+41:30:30.5	3.79	AC0316	1992-12-16	1.59	3208	2002-09-25	149.3
				AC0316	1992-12-16	4.74	4379	2002-09-26	
4C +60.07	05:12:55.177	+60:30:50.8	3.79	AI88	2001-10-19	24.0	10489	2008-12-10	100.2
				AC0374	1994-03-18	4.74			
TN J1338−1942	12:38:26.1	−19:42:31.1	4.11	AD398	1997-01-25	4.86	5735	2005-08-29	78.7
							6367	2005-08-31	
							6368	2005-09-03	
4C +63.20	14:36:37.326	+63:19:13.1	4.26	AC0374	1994-03-18	4.74	18106	2017-06-14	99.1
				AB870	1998-08-17	4.89	19954	2017-03-13	
							20033	2017-03-11	

Notes. Positions and redshifts are from the NASA/IPAC Extragalactic Database (NED).

Table 2. X-ray and Radio Parameters for the integrated emission.

Name	Redshift	Position	$r_{\rm eff}$ (kpc)	$\log L_{\rm r}$ (erg s^{-1})	$\log L_{\rm X}$ (erg s^{-1})	$\log L_{\rm X,CMB}$ (erg s^{-1})
3C 469.1	1.336	N	67.2	44.09±0.02	43.71±0.07	44.63
		S	67.9	44.05±0.03	43.75±0.07	44.62
4C +39.24	1.883	E	86.2	43.27±0.06	44.19±0.07	44.83
		W	80.2	43.84±0.02	44.21±0.06	45.02
3C 9	2.02	NE	18.9	44.45±0.01	43.63±0.06	44.29
		SW	22.1	44.76±0.01	43.60±0.05	44.53
4C +23.56	2.483	NW	36.7	43.81±0.04	44.24±0.05	44.75
		SE	47.4	43.80±0.02	44.25±0.04	44.94
B3 0727+409	2.5	W	35.6	<42.80	44.52±0.03	44.32
4C +03.24	3.57	NE	12.2	44.01±0.05	44.12±0.13	44.49
		S	11.5	44.38±0.04	44.25±0.11	44.60
4C +19.71	3.59	N	12.1	44.33±0.01	43.70±0.20	44.63
		S	14.3	44.14±0.02	43.82±0.18	44.67
4C +41.17	3.79	NE	19.5	44.36±0.01	44.53±0.06	45.07
		SW	13.7	44.23±0.01	44.41±0.07	44.75
4C +60.07	3.79	E	11.8	44.05±0.01	43.88±0.16	44.57
		W	14.7	44.22±0.01	43.77±0.16	44.81
TN J1338−1942	4.11	N	8.2	44.26±0.01	43.92±0.18	44.50
		S	7.8	42.96±0.03	<43.64	43.90
4C +63.20	4.26	N	7.7	44.09±0.01	44.28±0.13	44.43
		S	6.9	44.60±0.01	44.10±0.16	44.57

Notes. $r_{\rm eff}$ is the radius of a sphere with the same volume as the emission region, assuming an axisymmetric, prolate spheroid. $L_{\rm r}$ and $L_{\rm X}$ refer to the measured radio and X-ray luminosity, respectively. $L_{\rm X,CMB}$ refers to the expected X-ray luminosity arising from IC/CMB (see Equation 4).
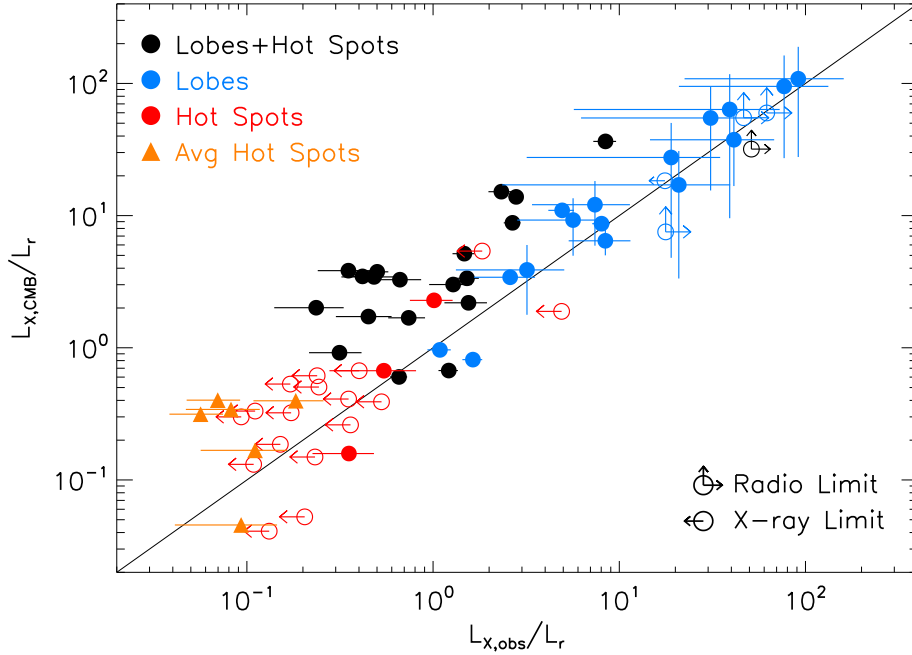
Figure 2. A comparison between the expected X-ray luminosity arising from IC/CMB in equipartition, $L_{\rm X,CMB}$, and the observed X-ray luminosity, $L_{\rm X,obs}$, each normalized by the measured radio luminosity, for the high-z radio galaxies under analysis. For each galaxy, the black points (total) refer to the integrated emission (that is, the lobes plus hot spots, excluding the core), while the red and blue points are measurements from the individual hot spots and lobes, respectively. Filled symbols represent sources detected in both the X-ray and radio bands, while open symbols refer to upper limits. Orange triangles represent mean hot spot values for systems where at least one hot spot is undetected. The upper right corner corresponds to large, weakly magnetized structures and the lower left corner to more compact, strongly magnetized structures. Whereas the lobes are scattered close to the solid line that indicates agreement between the IC/CMB equipartition model predictions and the observations, the total emission is systematically offset from it.

Table 3. X-ray and Radio Parameters for Lobes.

Name	Redshift	Side	$r_{\rm eff}$ (kpc)	$\log L_{\rm r}$ (erg s^{-1})	$\log L_{\rm X}$ (erg s^{-1})	$\log L_{\rm X,CMB}$ (erg s^{-1})	$B_{\rm eq}$ (μG)	$\tau_{\rm sync}$ (Myr)
3C 469.1	1.336	N	34.2	42.80±0.31	43.67±0.09	43.89	5.3	106
		S	30.2	42.91±0.27	43.66±0.09	43.87	6.1	86
4C +39.24	1.883	E	74.05	42.34±0.54	44.23±0.07	44.32	2.9	263
		W	74.1	42.25±0.59	44.21±0.08	44.28	2.7	293
3C 9	2.02	NE	18.9	44.32±0.01	44.53±0.06	44.23	34.4	6.4
		SW	22.1	44.40±0.01	44.43±0.07	44.38	31.6	7.3
4C +23.56	2.483	NW	36.7	42.94±0.76	44.22±0.05	44.38	7.9	59
		SE	47.4	42.64±0.82	44.24±0.04	44.45	5.2	110
B3 0727+409	2.5	W	35.6	<42.52	44.31±0.04	44.04	<7.1	>69
4C +03.24	3.57	NE	8.3	<42.81	44.06±0.14	43.69	25.9	9.9
		S	11.4	43.74±0.34	44.25±0.11	44.33	36.1	6.0
4C +19.71	3.59	N	12.1	<42.03	<43.58	-	11.1	35
		S	14.3	<42.03	43.70±0.20	43.77	9.7	43
4C +41.17	3.79	NE	19.5	43.79±0.03	44.48±0.07	44.83	23.6	11
		SW	13.7	43.51±0.04	44.41±0.08	44.44	26.5	9.5
4C +60.07	3.79	E	11.8	42.20±0.35	43.82±0.18	43.78	12.8	28
		W	14.7	44.20±0.55	43.69±0.19	43.94	9.7	43
TN J1338−1942	4.11	N	8.2	42.52±0.71	43.84±0.20	43.75	21.5	13
		S	7.8	42.40±0.83	<43.64	43.66	20.7	14
4C +63.20	4.26	N	7.7	43.26±0.11	44.19±0.13	44.07	37.0	5.8
		S	6.9	43.60±0.04	44.02±0.19	44.14	50.9	3.6

Notes. Same notation as in Table 2 for $L_{\rm X}$ and $L_{\rm r}$. $\tau_{\rm sync}$ is calculated at 1 GHz.

Table 4. X-ray and Radio Parameters for Hot Spots.

Name	Redshift	Side	r_{eff} (kpc)	$\log L_{\text{r}}$ (erg s^{-1})	$\log L_{\text{X}}$ (erg s^{-1})	$\log L_{\text{X,CMB}}$ (erg s^{-1})	$\log L_{\text{X,SSC}}$ (erg s^{-1})	B_{eq} (μG)
3C 469.1	1.336	N	15.9	44.07±0.02	<43.04	43.55	42.84	33.9
		S	16.1	44.01±0.01	<43.06	43.53	42.74	32.3
4C +39.24	1.883	E	27.6	43.18±0.04	<43.45	43.92	41.28	12.2
		W	27.4	43.83±0.01	43.83±0.13	44.19	42.29	18.7
3C 9	2.02	NE	5.0	43.89±0.01	<43.30	43.06	43.90	80.4
		SW	8.4	44.50±0.01	43.61±0.20	43.71	43.71	78.0
4C +23.56	2.483	NW	6.8	43.75±0.05	<42.98	43.47	42.34	56.6
		SE	3.7	43.77±0.02	<42.95	43.04	42.56	95.8
B3 0727+409	2.5	W	12.3	<42.16	44.11±0.07	43.27	40.14	<12.2
4C +03.24	3.57	NE	3.5	43.91±0.02	<43.46	43.52	42.80	111.2
		S	2.9	43.72±0.02	<43.45	43.31	42.56	113.9
4C +19.71	3.59	N	<1.2	44.32±0.01	<43.44	42.94	43.77	>354.6
		S	<1.2	44.13±0.02	<43.44	42.85	43.47	>312.7
4C +41.17	3.79	NE	<3.8	43.79±0.29	43.53±0.01	43.62	42.82	>95.4
		SW	<3.8	43.79±0.01	<43.39	43.62	42.82	>95.4
4C +60.07	3.79	E	3.9	44.05±0.01	<43.44	43.75	43.23	109.8
		W	3.4	44.20±0.01	<43.44	43.71	43.51	312.7
TN J1338−1942	4.11	N	4.2	44.18±0.01	<43.56	43.97	43.16	113.3
		S	2.9	42.82±0.03	<43.51	43.10	41.15	65.0
4C +63.20	4.26	N	<2.2	44.07±0.01	<43.63	43.49	43.20	>184.9
		S	<2.2	44.59±0.01	<43.63	43.71	44.02	>260.0

Notes. Same notation as in Table 2; $L_{\text{X,SSC}}$ is the expected X-ray luminosity arising from synchrotron-self-Compton (based on the SSC emissivity expression given in Equation 7).

Table 5. X-ray and Radio Parameters for Averaged Hot Spots.

Name	Redshift	r_{eff} (kpc)	$\log L_{\text{r}}$ (erg s^{-1})	$\log L_{\text{X}}$ (erg s^{-1})	$\log L_{\text{X,CMB}}$ (erg s^{-1})	$\log L_{\text{X,SSC}}$ (erg s^{-1})
3C 469.1	1.336	16.0	44.05±0.01	42.80±0.56	43.54	42.54
4C +23.56	2.483	5.3	43.76±0.03	42.67±0.71	43.29	42.43
4C +03.24	3.57	3.8	43.83±0.01	43.09±0.86	43.43	42.88
4C +19.71	3.59	<1.2	44.24±0.01	43.21±0.31	42.90	43.64
4C +60.07	3.79	3.7	44.13±0.01	42.97±0.55	43.73	43.13
4C +63.20	4.26	<2.2	44.41±0.01	43.45±0.49	43.63	43.72

Notes. Average values are reported for systems where the hot spots are individually undetected in the X-rays, but for which adding up counts from hot spots on both sides of the core leads to a significant detection. The same notation is used as in Table 2 and 3.

3.4 Measurement Regions

Most of the systems included in this study are double-lobed radio galaxies much larger than the Chandra point-spread function, so we make measurements on both sides of the core. We ignore or mask the core, and measure the total L_{X} and L_{r} on each side, as well as in the lobes and hot spots separately. The measured values are reported in Tables 2, 3 and 4. The 1σ error bars are purely statistical and do not account for error in redshift, region, size, spectral index, etc.

To determine the sizes and locations of the lobe and hot spot regions we use interferometric VLA radio images. If possible, we use the lowest frequency and multiple images with different resolutions to estimate the lobe extent, as the diffuse lobe emission could be resolved out in extended VLA arrays. In several cases, there is little lobe structure visible in any existing image (Figure 1) and so we supplement with the X-ray images themselves and define the outline of the lobe region based on the extent of the X-ray surface brightness. In the event that the lobes are not clearly defined in the radio or X-ray, we demarcate their extent by the position of the outermost hot

spots, which are presumed to trace terminal jet shocks, and on the sides by the extent of radio or X-ray emission (see discussion of this choice in Section 4). We exclusively use ellipses and assume that the volumes are prolate and axis-symmetric spheroids with effective radius r_{eff}. This choice is necessarily subjective and does not reflect the complex volumes sometimes seen in more local radio galaxies. It is also possible that there are more extended lobe structures only visible at low frequencies due to spectral ageing. The impact of these assumptions is discussed in § 4.3.

We followed a similar procedure to measure the sizes of the hot spots, which are usually very well defined in the radio. In some high-z radio galaxies there are multiple hot spots, and here we restrict our analysis to the outermost hot spots (although we mask all hot spots when measuring the lobe emission). For these hot spots, if the source is resolved then we use an aperture based on the contour. Otherwise, we determine whether the hot spot is pointlike in the highest resolution image available by comparing the flux between images of different beamsizes. If little or no flux is resolved out at

higher resolution, we use the smallest beamsize as the upper bound on the hot spot size and report the peak pixel flux in Jy (since the maps are calibrated in Jy bm^{-1}). The hot spot regions are frequently comparable to or smaller than the ACIS half-power diameter of 0.8 arcsec. In this case, we treat the hot spot as an X-ray point source and measure the number of counts within a 2 arcsec diameter circle centered on the hot spot. We likewise use this value to estimate the X-ray flux from the lobes (i.e., subtract out any hot spot or point-like emission). However, to calculate the predicted X-ray luminosity we use the "true" volume from the radio.

The reported X-ray luminosities are not corrected for the fraction of each lobe covered by the hot spots. If we assume uniform surface brightness, the correction factors are between 1-10%, except in the northern lobe of TN J1338−1942, where the correction factor is about 40%. Not including this prediction may lead to systematically lower $L_{\mathrm{X,obs}}$ relative to the predicted $L_{\mathrm{X,CMB}}$, but as the lobes may not have uniform surface brightness the true correction factor may be larger or smaller. Regardless, not adjusting $L_{\mathrm{X,obs}}$ upwards does not substantially affect our results.

Because $B_{\mathrm{eq}} \propto r^{12/7}$, the uncertainty in the volume is a large source of uncertainty in comparing the observed and predicted X-ray luminosities. It is also possible that the volume filling factor of the lobes is substantially less than unity, at least for relativistic cosmic rays, as low redshift, FR II radio galaxies frequently show plasma flowing back from the terminal shocks into the lobes with jellyfish-like structures. If we have overestimated the volume, the effect is to over-predict the X-ray luminosity for a given radio luminosity. We return to this in Section 4.

3.5 Comments on individual high-z radio galaxies

3.5.1 *3C 469.1, 4C +39.24, 4C +23.56, 4C +60.07, TN J1338−1942*

These are classical Fanaroff-Riley (FR) Type II (Fanaroff & Riley 1974) radio galaxies with no visible jet, weak lobe emission, and very bright hot spots. We define the lobe region based on the extent of the hot spots and the apparent width of the X-ray emission associated with the galaxy, which leads to long, narrow lobes.

3.5.2 *3C 9*

This is a classical double radio galaxy with bright radio lobes that neatly match up with the enhanced X-ray emission. The hot spots are defined based on high frequency images, whereas the lobe extent is taken from a 1.55 GHz image.

3.5.3 *B3 0727+409*

Simionescu et al. (2016) discovered this high-z radio galaxy in the X-rays, as it has no diffuse radio counterpart (it does have a radio core and knot in the same direction as the extended X-rays). The X-ray structure is consistent with a jet and a diffuse lobe, so we define the lobe as the region outside of the inner jet. There is an X-ray bright region at the end of the lobe that we identify as a hot spot, but with no radio emission this classification is questionable. In the following analysis, we treat the region as a hot spot, but if we instead treat the entire system as a lobe it does not alter our conclusions.

3.5.4 *4C +03.24*

The best interferometric images of 4C +03.24 show diffuse radio emission beyond the hot spots, but the size of any lobe cannot be reliably measured. Thus, we base the size of the lobe on the smoothed X-ray image, shown in Figure 1. This leads to some uncertainty on the X-ray flux and volume for the lobe beyond that reported in Table 3, but it is clear that the X-ray emission extends beyond the bright radio contours.

3.5.5 *4C +19.71*

This high-z radio galaxy has bright hot spots and no significant lobe emission. The X-ray emission appears to be extended beyond the hot spots, and so we define the lobes based on the apparent X-ray enhancement. We note that Wu et al. (2017) found no statistically significant evidence for diffuse X-ray emission around the core using circular annuli, but along the axis joining the hot spots there is a significant detection. However, this is only true when summing the north and south lobe regions, and it is not clear whether the cluster of X-ray counts to the south is part of the radio galaxy. Of the radio galaxies our sample, the measurements are least secure for 4C +19.71.

3.5.6 *4C +41.17*

There is bright X-ray emission on both sides of the core, but to the northeast the hot spot is very close to the core, with diffuse emission beyond. It is not clear whether the northeast hot spot is truly a terminal shock, but as the radio lobe is well defined and overlaps the X-ray enhancement well (see also Wu et al. 2017), we define the lobe region based on the radio contours.

3.5.7 *4C +63.20*

This system was recently studied by Napier et al. (2020), who determined that there is significant X-ray emission associated with the lobes. We define the extent of the X-ray lobes based on their work and their apparent width, but note that the radio emission allows for narrower lobes.

4 RESULTS

We began by computing the expected L_{X} from IC/CMB in equipartition, $L_{\mathrm{X,CMB}}$, following Equation 4, for each of the high-z radio galaxies. The predicted total values, i.e. when the total (lobes+hot spot) volume and radio luminosity were used, are given in Table 2, whereas the predicted values for the hot spots and lobes separately are given in Tables 3 and 4. Most of the hot spots are not detected in the X-rays at the 3σ level, but in several systems there are counts in each of the hot spot regions, so we also compute an average value for those systems where stacking the hot spot regions across the core leads to a detection, using the same regions as defined above. The average measured luminosities, and predicted $L_{\mathrm{X,CMB}}$ values for those are given in Table 5.
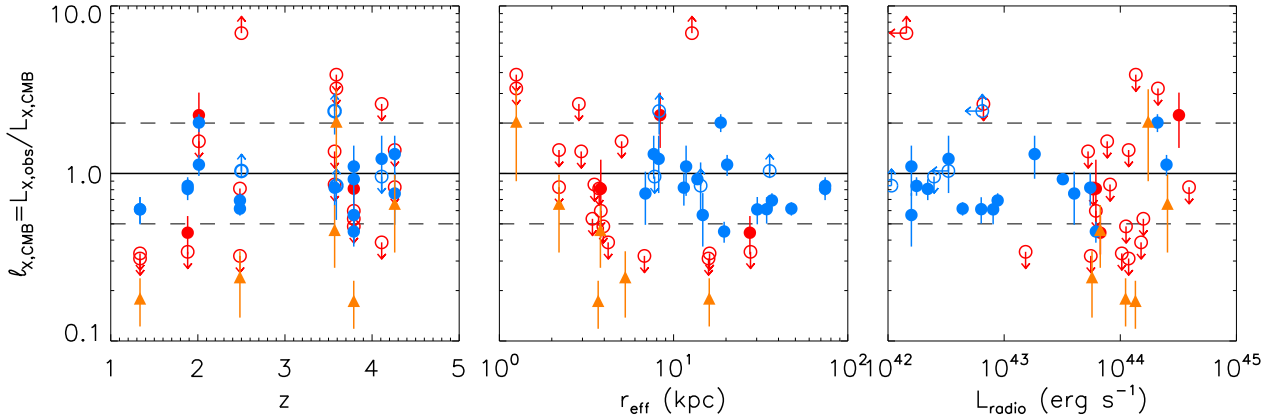
Figure 3. The ratio $L_{X,obs}/L_{X,CMB}$ for high-z radio galaxies, plotted against redshift (*left*), emitting region size (center), and measured radio luminosity (*right*). Symbols are the same as in Figure 2, except that only the decomposed hot spots and lobes are shown. The measured luminosities of the lobes are within a factor of two (marked by the dashed lines) of the expected IC/CMB equipartition value. There is no significant correlation between the observed/predicted L_X and any parameter. The lobes of high-z radio galaxies with a wide range of physical sizes and luminosities are near equipartition.

4.1 Testing IC/CMB in equipartition

Figure 2 compares the observed X-ray emission, $L_{X,obs}$, to the predicted X-ray luminosity arising from IC/CMB in equipartition, $L_{X,CMB}$, each normalized by the measured radio luminosity. The black points (total) represent measurements from the entire radio galaxy (minus the core when present), while blue and red points represent the contribution from the individual lobes and hot spots, respectively. Most lobes are detected in both X-rays and radio emission, albeit with some ambiguity as to what is true lobe emission (as opposed to a radiative jet or a faint hot spot complex). The southern lobe of TN J1338−1942, which is not detected in X-rays, corresponds to an upper limit to the $L_{X,obs}/L_r$ ratio. Meanwhile, the lobe of B3 0727+409, the northeast lobe of 4C +03.24, and the southern lobe of 4C +19.71 are not detected in the radio, so we compute lower limits to the $L_{X,obs}/L_r$ and $L_{X,CMB}/L_r$ ratios. The northern lobe of 4C +19.71 is not detected in X-rays, nor in radio, and is thus omitted from the plot. Only three hot spots have both radio and X-ray detections.

The observed (radio-normalized) X-ray emission from the lobes+hot spots is typically lower than predicted from IC/CMB, with a median observed-to-predicted ratio ($\ell_{X,CMB} \equiv L_{X,obs}/L_{X,CMB}$, see also Figure 3) of 0.29; this result is fully consistent with previous investigations (e.g., Smail et al. 2012; Smail & Blundell 2013), and indicates that either the lobes, or the hot spots, or both, are off of (and specifically sub-) equipartition.

Emission from the lobes alone is consistent with $\ell_{X,CMB} = 1$, with a median value of 0.84. Incidentally, the median value for the lobes is similar to the average $\ell_{X,CMB} \simeq 0.7$ measured at lower redshift for powerful radio galaxies (Croston et al. 2005; Kataoka & Stawarz 2005; Worrall 2009). Although most hot spots are not individually detected in X-rays, the distribution of the limits implies that $\ell_{X,CMB} < 1$ in most of them. When considering the averaged hot spot values (orange triangles) along with individually detected hot spots, we find a median $\ell_{X,CMB}$ of 0.46, indicating that the hot spots are off of equipartition. However, as we discuss in the following subsection, it is not clear that we can conclude this because SSC is expected to contribute significantly to–possibly

dominate–the X-ray emission in hot spots, and there may also be a second synchrotron population contributing to the X-rays. It is also possible that a failure to measure equipartition is due to offsets between the X-ray and radio peaks for a given hot spot, which can be significant fraction of an arcsecond and likely result from relativistic shocks (Hardcastle et al. 2004, 2007)

In light of this analysis, we argue that the lobes of the high-z radio galaxies are fully consistent with the expectations from a IC/CMB model in equipartition. Previous claims to the contrary are typically based on luminosity measurements of the aggregated, lobe+hot spot regions, and such measurements are not usually appropriate, as interpreting the aggregate relies on a precise understanding of each component. Instead, a fair comparison between theory and observations requires substituting the relevant (i.e. lobe vs. hot spot) luminosities as well as sizes in Equation 4. This can only be achieved for high-quality data which allow for a proper decomposition.

Figure 3 also illustrates that there is no significant correlation (at the 95% confidence level) between $\ell_{X,CMB}$ and the redshift, effective radius, or radio luminosity of the high-z radio galaxies under analysis. This is true of either the hot spots or the lobes, when considering limits as well as detected systems. The test is warranted, since, given a sufficiently large sample that includes very large systems ($r_{eff} > 100$ kpc, i.e., in the realm of giant radio galaxies), we would expect to see an anti-correlation between $\ell_{X,CMB}$ and r_{eff}. This is because the predicted scaling of $L_{X,CMB}$ with $r_{eff}^{12/7}$ assumes a uniform filling factor and magnetization. These assumptions are unlikely to hold for very large systems even if the *emitting volume* is roughly in equipartition. However, we do not see this effect in the sample.

To summarize, Figures 2 and 3 show that (i) the lobes of the high-z radio galaxies considered in this work are consistent with IC/CMB at or near equipartition, and (ii) there is no indication that this changes with redshift, AGN power, or lobe size.

4.2 The role of Synchrotron Self-Compton

SSC emission, whereby the relativistic electrons also cool by IC scattering off of the same population of photons that they produce via synchtotron, is expected to be important in the compact, highly magnetized hot spots. Thus, it is not surprising that $\ell_{X,CMB} < 1$ for most hot spots in our sample, since the X-rays are likely not predominantly IC/CMB.

Since the SSC X-ray luminosity, $L_{X,SSC}$, also depends on B, we can test whether $B \approx B_{eq}$ in the hot spots with this definition. To calculate the equipartition $L_{X,SSC}$, we need to know both the number of seed photons (estimated from the radio luminosity) and the optical depth to Compton scattering, $\tau = \sigma_T N_0 r$, where N_0 is the number density of electrons, and r is the characteristic path length, which we take to be the radius of a uniform sphere. In equipartition, $u_B = (1 + k)u_e$, where $k = 0$ is the ratio of energy in non-radiating particles to electrons, $u_B = B_{eq}^2/8\pi$, and

$$u_e = \int EN(E)dE = \int E(N_0 E^{-p})dE = N_0 m_e c^2 \int_{\gamma_{min}}^{\gamma_{max}} \gamma^{1-p} d\gamma \quad (6)$$

where we have assumed a power law distribution of electron energies between $\gamma_{min} = 10$ and $\gamma_{max} = 10^4$, with index $p = 2$ (i.e., exactly the same assumptions as for IC/CMB). Thus, we can solve for N_0 in terms of B_{eq}.

The synchrotron emissivity is a power law between the rise and break regions, with $J_s(\nu) = J_{0,s}\nu^{-\alpha}$, where $\alpha = (p - 1)/2$. The emissivity has units erg s^{-1} cm^{-3} Hz^{-1} sr^{-1}, so we can find $J_{0,s}$ from the measured L_r at a given frequency and the hot spot size, which is converted to an effective spherical radius. The SSC emissivity can then be written ([Ghisellini 2013](#)):

$$J_{ssc}(\nu) = \left(\frac{4}{3}\right)^{\alpha-1} \frac{1}{2}\tau J_{0,s}\nu^{-\alpha} \int_{\nu_{min}}^{\nu_{max}} \nu^{-1} d\nu \quad (7)$$

We convert this back to a 2-10 keV X-ray luminosity for comparison with the data (Table 4).

When comparing the observed X-ray luminosity to $L_{X,SSC}$ for the hot spots in our sample (Figure 4), the individual detections and limits (red circles) are broadly scattered around the expected equipartition value $\ell_{X,SSC} \equiv L_{X,obs}/L_{X,SSC} \simeq 1$, and the average hot spot measurements (orange triangles) are consistent with equipartition. The hot spots are also consistent with the trend found by [Hardcastle et al. (2004)](#) for low-z systems that the discrepancy between the observed $L_{X,obs}$ and equipartition $L_{X,SSC}$ is a function of radio luminosity. Figure 4 shows their measurements in grey and ours in red/orange. The hot spots from the high-z radio galaxies are at the high radio luminosity end (at least in part due to selection effects), but they follow the same basic trend as the lower z sample. This is particularly clear for the average hot spot values (i.e., those systems where we detected the hot spots in X-rays when stacking the two regions on either side of the core), which are shown as orange triangles.

To summarize, our analysis shows that both the lobes and hot spots of high-z radio galaxies appear to be consistent with equipartition, and the hot spots (where the contribution from SSC is important in X-rays) are similar to the most luminous systems studied at lower redshift. In other words, the high-z radio galaxies under examination are not unusual in their behaviour as radio galaxies.
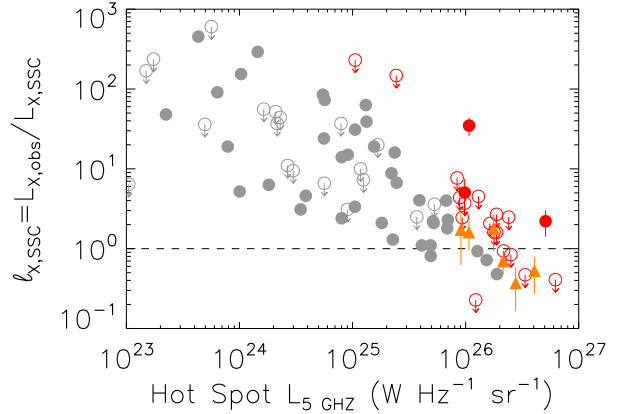

Figure 4. A comparison between the expected X-ray luminosity arising from SSC in equipartition, $L_{X,SSC}$, and the observed X-ray luminosity, $L_{X,obs}$, for a sample of radio galaxy hot spots. The grey points are from the low-z sample of [Hardcastle et al. (2004)](#), while the red points are the high-z radio galaxies in this work. As in previous figures, the orange triangles represent the average values for pairs of opposing hot spots for systems in which the individual hot spots are not X-ray detected. The expected SSC luminosity was predicted following [Hardcastle et al. (2004)](#), using the measured radio luminosity and emitting region size and assuming equipartition. The high-z radio galaxies in our sample are broadly consistent with the [Hardcastle et al. (2004)](#) sample and with being close to equipartition.

4.3 Impact of assumptions

We make several assumptions when measuring L_r, r_{eff}, and $L_{X,obs}$. First, we assume that the lobes are ellipsoids with a filling factor of unity, and that the volume can be measured from the radio or X-ray surface brightness contours. A similar assumption applies to the hot spots. Secondly, we assume that there is negligible dimming of L_r, such that it is useful to calculate B_{eq}. Thirdly, we assume the same spectral index $\alpha = 1$ in all systems. Lastly, our estimate of B_{eq} assumes that the observed νL_ν represents all of the particles contributing to the energy density. We address the impact of (the uncertainty in) these assumptions on our results in turn below.

$L_{X,CMB}$ depends on $r_{eff}^{12/7}$, but the measured L_r and $L_{X,obs}$ also depend on the projected area of the lobe, so the effects largely cancel out if the lobe emission is approximately uniform. Despite the low numbers of counts in the lobes, most of the X-ray lobes have close to uniform surface brightness. Since the lobe regions are defined based on the surface brightness of the radio or X-ray emission, it is not likely that the regions we adopted are too small. However, they may be too large, with ellipses whose r_{eff} differ by 25-30% consistent with the data in several cases. This would lead to a 15% error in $\ell_{X,CMB}$. A similar uncertainty is incurred if the lobes are oblate, rather than prolate spheroids, but in the opposite direction. This amount of uncertainty does not change our conclusions.

The other uncertainty in the volume is the filling factor, ϕ, but as this uncertainty is related to the particle composition of the jet (i.e., whether there is a significant hadronic component), it pertains to the entire measurement scheme and should not be considered in isolation.

One of the objectives of this work is to examine whether

IC/CMB cooling can dim radio lobes at high redshift, in which case the measured L_r can be smaller than what would be expected for a given B_{eq}. Since we derive B_{eq} from L_r, this would erroneously decrease $L_{X,CMB}$ by a factor of $L_r^{2/7}$. Since $\ell_{X,CMB}$ explicitly contains the $(1 + z)^4$ effect and $\ell_{X,CMB}$ is not (further) correlated with z (Figure 3), we can conclude that any dimming must not be severe, with the caveat that it would be most prominent for the few systems at the largest z. Dimming consistent with the lack of correlation (by up to a factor of two at high z) would reduce $\ell_{X,CMB}$ to $\approx 75\%$ of its nominal value, so this would not qualitatively change our conclusions.

Thirdly, we have assumed that $\alpha = 1$ in each source for calculating L_r. This is a reasonable approximation for many steep-spectrum radio sources, but there may be significant dispersion. Since the radio sources are unresolved below 1 GHz and there are generally too few X-ray counts to robustly constrain α from the X-rays, we cannot directly test whether $L_r \simeq \nu L_\nu$ in the GHz band is a good approximation for each source. However, based on the unresolved radio SEDs of sources with weak radio cores[2], only a few sources show any evidence for a synchrotron break below 1 GHz, in which case $\alpha \approx 1$ is a good approximation.

We can estimate the impact of not knowing α in each source. Since the systems are high-z radio galaxies and we focus on extended components, we can place a lower bound of $\alpha = 0.7$. Meanwhile, no source appears to have $\alpha \gtrsim 2$, so we expect that $0.7 < \alpha < 2$, where these are conservative limits. If $\alpha = 0.7$ instead of 1, the rest-frame L_r is 40% of the reported value, which in turn leads to a factor of 1.5 higher (true) ℓ_X. If $\alpha = 2$ instead of 1, the true ℓ_X is 0.7 times the reported value. We do not expect the high-z radio galaxies here to be predominantly towards one end or the other of this range, and so uncertainty in α will manifest as an overall uncertainty in $L_{X,CMB}$ of about 40%. This would not change our conclusions, and indeed if treated as an "error bar" that can be added in quadrature with the statistical uncertainty, would have a small impact on the appearance of Figure 5; however, since this uncertainty cannot be treated in this way, it is not included in that figure.

Lastly, we have assumed in calculating B_{eq} that L_r represents the extent of the particles in each system, i.e., that γ_{min} and γ_{max} are based on the radio emission. This is not the case, so it is likely that B_{eq} is underestimated, especially for steep-spectrum sources (although we do not know the true γ_{min} and γ_{max}). We use B_{eq} to estimate the predicted $L_{X,CMB}$, but in order to compare our derived B_{eq} values with those in the literature, Tables 3 and 4 include them. In the lobes, the values range from 2–50 μG, which is similar to the field strengths measured in more nearby samples using different techniques (Croston et al. 2005; Bîrzan et al. 2008; Harwood et al. 2016), and where similar radio–X-ray analyses have been carried out (e.g., Croston et al. 2005). This suggests that our assumption does not significantly affect our conclusions.

Another way to consider the same issue is to calculate the γ probed at 1 GHz from B_{eq}, using $\gamma \approx \sqrt{\nu/\nu_G}$. The electron gyrofrequency is $\nu_G \approx 2.8B[\mu G]$ Hz. 2,000 and 11,000, with an average near 4,000. This is near the upper end of the range frequently used in the literature, $10 < \gamma < 10^4$, so for steep-spectrum sources B_{eq} may indeed be underestimated. If we adopt an initial electron energy power-law index of 2, we expect B_{eq} to be higher by 10-40%

---

in the different lobes than our calculated values, based on the γ that produces 1 GHz emission. Since we do not know the true range nor the electron energy distribution, it is not clear whether or how much this estimate is better, but it does not substantially alter our conclusions.

A related issue is that the X-ray bright sample observed by Chandra is likely biased towards very active sources, so that CMB cooling may not have had enough time to quench the system (i.e., the replacement rate of energetic particles is very high). We calculated the synchrotron lifetimes based on our B_{eq} values (see Table 3 for the lobes, calculated at 1 GHz):

$$\tau_{sync} = \frac{m_e c^2}{\frac{4}{3}\sigma_T c U_B \gamma} \tag{8}$$

The values range from 3-300 Myr, reflecting the strong dependence on the lobe size (on which our inferred B_{eq} depends). There is no significant correlation between the observed L_X or L_r and the projected lobe size, nor between the core luminosities and B_{eq}, so there is no clear preference for especially active sources in the sample. Although the sample presented here is small and biased towards X-ray bright sources, the similarity to low-redshift radio galaxies in terms of size and B_{eq} indicate that it is a reasonable sample in which to test the CMB-quenching hypothesis.

5 DISCUSSION

5.1 IC/CMB X-ray brightening

Motivated by the mandatory increase in the expected IC/CMB X-ray luminosity at higher redshift, as $u_{CMB} \propto (1 + z)^4$, previous works have searched for a correlation between $L_{X,obs}/L_r$ and z (Section 1). However, here we wish to emphasize that, if high-z radio galaxies are in equipartition, then one does not expect $L_{X,obs}/L_r$ to strongly correlate with z even though CMB X-ray brightening does occur. This is for two reasons: first, as we showed, any such correlation can be washed out when comparing entire radio galaxies, for which (at high redshift) most X-rays come from the lobes and most radio emission comes from the strongly magnetized jets or hot spots. Secondly, even in lobe-dominated sources, and/or if the emission from the hot spots is thoroughly excluded, $L_{X,CMB}$ depends also on L_r and size, as $L_r^{3/7}$ and $r^{12/7}$, respectively. Figure 5 illustrates this point by plotting $L_{X,obs}/L_r$ for only the lobes in our sample, in the left panel, and a scaled version of Equation 4, in the right panel. The lines are arbitrarily scaled functions of $(1 + z)^4$ and are not fits to the data. One can clearly see that, even within the lobes, $L_{X,obs}/L_r$ is not strongly correlated with redshift, whereas the function in the right panel shows remarkable agreement with the expectations from IC/CMB in equipartition, where the measured $(L_{X,obs}/L_r^{3/7} r_{eff}^{12/7})$ values for the lobes are consistent with a $(1 + z)^4$ scaling up to $z \gtrsim 4$.

In essence, this proves that, when decomposed into lobes and hot spots, the high-z radio galaxy radio and X-ray data are fully consistent with a picture where synchrotron cooling in the lobes is progressively offset by IC scattering of CMB photons, which in turn causes the lobes to brighten in the X-rays, and become dimmer in the radio band. This also implies that there is no need for an additional FIR photon field to explain the observed $L_{X,obs}/L_r$ in the lobes of this sample, which overlaps the sample from Smail & Blundell (2013) where this solution was explored (even though we
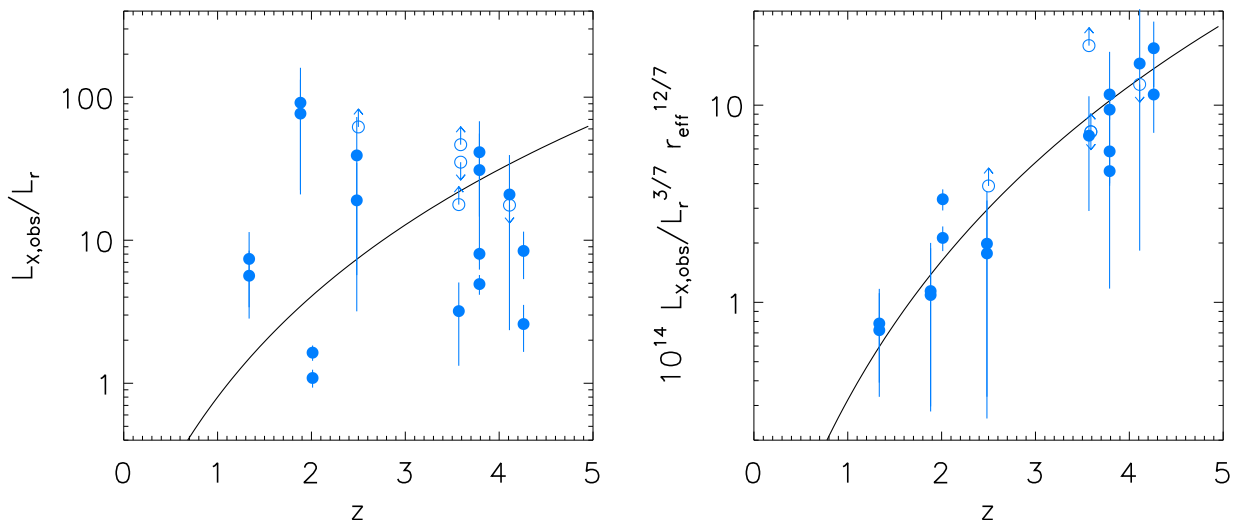
Figure 5. Even in equipartition, we do not expect $L_{X,obs}/L_r$ to correlate strongly with z in small samples, because L_X also depends on B^2, which depends on the lobe size (see Equation 4). *Left*: $L_{X,obs}/L_r$ as a function of z for the resolved lobes of the target high-z radio galaxies. Open circles are upper limits. *Right*: Scaled $L_{X,obs}/(L_r^{3/7} r_{eff}^{12/7})$ as a function of z, for the same lobes. This is a re-projection of Figure 2, as the exponents on L_r and r_{eff} are those in Equation 4. In both panels, the solid line is proportional to $(1 + z)^4$ and arbitrarily scaled. It is not a fit, but clearly the points in the right panel are more consistent with this scaling, and they are at least strongly correlated with z.

cannot rule out that IC/FIR does contribute a fraction of the X-rays from these data).

An additional reason that surveys of high-z radio galaxies may not find a correlation between $L_{X,obs}/L_r$ and z is that the X-ray emission in a significant fraction of these systems with Chandra data is dominated by jets (which were not included in our sample). There is evidence for IC/CMB dominated jets (Worrall et al. 2020; Schwartz et al. 2020), as well as X-ray synchrotron emission (Meyer et al. 2015). As with SSC emission in the hot spots, a second, more energetic population of electrons that radiates X-ray synchrotron emission will not depend on redshift. Hence, CMB brightening may not be detectable from $L_{X,obs}/L_r$ even with a much larger sample of resolved high-z radio galaxies than currently exists.

5.2 IC/CMB radio quenching?

The $(1 + z)^4$ dependence of the IC/CMB effect has been invoked to explain the apparent dearth of luminous radio-loud AGN at $z \gtrsim 3$ (Volonteri et al. 2011). This work started by estimating the fraction of radio-loud objects amongst all FIRST[3]-detected SDSS[4] quasars (defined as AGN with bolometric luminosities exceeding 10^{47} erg s^{-1} in the seventh data release), in different redshift bins. This fraction was then (i) normalized to the radio-quiet quasar luminosity function derived by Hopkins et al. (2007), to obtain the total number of radio-loud quasars per redshift bin between $1 \lesssim z \lesssim 6$, and (ii) compared to the expected number of massive radio galaxies (with estimated black hole masses in excess of 10^9 solar) starting from the parent blazar population. The latter was derived by normalizing the number of blazars inferred from those detected in the three-year Swift-BAT[5]

sample (Ajello et al. 2009) to the "minimal" blazar luminosity function derived by Ghisellini et al. (2010), then multiplied by a factor $2\Gamma^2$, where Γ is the bulk Lorentz factor of the jet, to account for the misaligned sources. This analysis found agreement between the expected and observed numbers up to $z \simeq 3$, above which the number of observed systems appears to drop sharply, with as many $500 - 5200(5200 - 7800)$ sources expected in the $5 - 6(4 - 5)$ redshift bin, vs. only $56(252)$ identified/detected, assuming $\Gamma = 15$.

Taking these numbers at face value, Ghisellini et al. (2014) and Ghisellini et al. (2015b) explored the possibility of IC/CMB radio quenching, whereby IC/CMB becomes more effective than synchrotron cooling at high-z, thus causing radio dimming (at rest-frame GHz frequencies) to below the 1 mJy sensitivity of the FIRST survey. They did so by fitting the spectral energy distributions (SEDs) of a sample of blazars at $z > 4$ with components for the accretion disk, beamed jet, and torus, then assessing the amount of lobe and hot spot emission allowed under equipartition. They concluded that IC/CMB quenching is possible when the kinetic luminosities of the hot spots and lobes are 1% that in the jet, which is consistent with the radio data for their sample. In this case, hot spot emission is too weak (at 1.4 GHz) to be detected, and the lobes can be quenched by IC/CMB.

Although the high-z radio galaxies in our sample are at systematically lower redshifts, they are very similar to the misaligned counterparts expected for the high-z blazars discussed in Ajello et al. (2009) and Ghisellini et al. (2015b). Their bolometric luminosities are between 10^{46} and 10^{48} erg s^{-1} (assuming a 2–10 keV bolometric correction factor of 50 for the core; Vasudevan & Fabian 2007), which places them in the same regime as the high-z blazars studied by Ghisellini et al. (2015b). In this work, we also find that they are close to equipartition and that they appear to be very similar to low-z radio galaxies. Meanwhile, Ghisellini et al. (2015b) concluded that $z > 4$ blazars are consistent with equipartition and that they

---

[3] Faint Images of the Radio Sky at Twenty-cm.
[4] Sloan Digital Sky Survey.
[5] Burst Alert Telescope.

are similar to lower redshift blazars. Taken together, these findings indicate that the high-*z* radio galaxies presented here are indeed misaligned blazars in the same regime as those in Ghisellini et al. (2015b).

Nevertheless, most of the high-*z* radio galaxies in our sample have hot spots with radio luminosities exceeding 10^{43} erg s^{-1}; as shown below, these cannot be quenched at $z < 5$ (this was already discussed for a few of the systems in our sample, by Wu et al. 2017 and Napier et al. 2020). For a hot spot with radius 2 kpc, 10^{43} erg s^{-1} corresponds to $B_{\rm eq} \simeq 100\ \mu$G, whose magnetic energy density is in equipartition with the CMB at $z = 5$. Thus, no significant dimming will occur until higher redshifts. Meanwhile, the FIRST sensitivity of $\simeq 1$ mJy at 1.4 GHz corresponds to 4×10^{42} erg s^{-1} at $z = 5$, so this hypothetical hot spot would be detected by FIRST. Almost all of the hot spots in our sample have higher $L_{\rm r}$ values, so they would be detectable as FIRST sources if they were observed at $z \gtrsim 5$. This suggests that, even if IC/CMB quenching of lobes occurs, to the extent that our sample is representative of high-*z* radio galaxies then IC/CMB quenching alone cannot explain the deficit of luminous, radio-loud quasars above $z \gtrsim 3$.

The main caveat with this statement is that the sample may not be representative: it consists of high-*z* radio galaxies observed with Chandra, and for which it is straightforward to decompose the lobes and hot spots (generally implying that, by construction, the lobes are visible, and not completely quenched). However, we note that we use VLA images with angular resolution $\lesssim 1''$ (as compared to $5''$ for FIRST), and the rms noise is frequently less than the 0.15 mJy of FIRST, so the decomposition presented here could not be achieved with the FIRST data. Regardless, the question is whether the *hot spots* in our sample are unusually luminous. For a comparison, we consider the catalog of low-*z*, FR II radio galaxies from the FIRST survey (Capetti et al. 2017). Most of those radio galaxies have well-defined hot spots that contribute a significant fraction of the GHz radio luminosity, implying that higher-redshift, jetted AGN are also likely to possess hot spots. For AGN with $L_{\rm bol} \gtrsim 10^{47}$ erg s^{-1}, these hot spots should typically be very luminous. We also note that Ghisellini et al. (2015b) do not robustly constrain $L_{\rm r}$ at rest-frame 1 GHz in the hot spots, and most of the blazars in their sample do allow for hot spots that could be detected by FIRST while remaining consistent with the fits to the SED of the AGN and beamed jet.

From this we are drawn to a second conclusion; whereas our work is consistent with IC/CMB quenching of most radio lobes at $z \gtrsim 4$, this effect would not be sufficient to explain the deficit of high-*z*, radio-loud AGN if such AGN frequently have bright hot spots, as suggested by our sample and a large number of low-*z* radio galaxies detected in the FIRST survey.

If IC/CMB is not responsible for making those radio galaxies "disappear", what then? Starting with the initial claim by Volonteri et al. (2011), several scenarios have been proposed–and largely dismissed–including a drop of the average jet bulk Lorentz factor at high-*z*, and the possibility that the SDSS misses a large fraction of high-*z*, radio-loud AGN because of extreme obscuration. Here, we briefly consider additional possible explanations, starting with the notion that most systems may not be in equipartition, and we only detect the small fraction that are. This, too, is not a very satisfying scenario because B must then be considerably smaller than $B_{\rm eq}$ in hot spots *except* for the ones that we can see, which resemble closer radio galaxies.

Alternatively, the high-*z* radio galaxies grow so large that the radio hot spots were not correctly associated with host galaxies. We note that the FIRST-detected quasars identified by Volonteri et al. (2011) are drawn from the Shen et al. (2011), who adopt a search radius of 30 arcsec to identify radio counterparts to any SDSS quasars within the FIRST footprint; this radius corresponds to a maximum physical size of $\lesssim 260$ kpc at $z = 1.4$ (above which the size starts to decrease because of cosmology). If a large fraction of the high-*z* radio-loud AGN were significantly larger than $\gtrsim 500$ kpc, they would have been missed. This hypothesis, too, is far-fetched. First, while such large radio galaxies do exist, they represent a small fraction of the nearby population. More to the point, for this effect to be at the root of the discrepancy, higher-*z* radio galaxies ought to be systematically larger than their nearby counterparts, which seems unlikely. It is worth noting that the average density of the Universe at $z \simeq 3$ is comparable to the typical intra-cluster density in a fully virialized, massive cluster at $z \simeq 0.5$, so the overall ambient density of high-*z* galaxies and their jets is not fundamentally different from their low-*z* analogs.

At the opposite end of the spectrum, most high-*z* radio galaxies could be very compact. Compact steep-spectrum and GHz-peaked sources (O'Dea 1998) are physically small (< 10 kpc), bright, radio galaxies that may be young systems. Such sources would not be easily quenched by the CMB, but radio galaxies about the same size as their host galaxies would be strongly cooled by their FIR radiation field (Smail & Blundell 2013). This scenario implies the existence of spatially resolved analogs at $z \lesssim 0.25$ (where Chandra could resolve their lobes), in which dusty starbursts have low radio emission and X-ray bright lobes. We briefly investigated the X-ray and radio emission from several ultraluminous infrared galaxies at low redshift (Tadhunter et al. 2011); these systems span a range of radio morphologies, sizes, and luminosities, but none of them are quenched, and none have notable IC/FIR X-ray emission. This cursory examination is not the final word, but once again demonstrates the challenge of explaining the lack of high-*z* radio galaxies through IC quenching from the starburst.

It also seems unlikely that jets are lower-power, preferentially hadronic, or disrupted, at high redshift. First, as noted in Section 1, it is counter-intuitive that the very powerful sources that produce high-*z* blazars produce very weak jets. Secondly, there is no systematic observational evidence for this (see, however, Spingola et al. 2020, who argue that the bulk Lorentz factor of the $z \simeq 6$ blazar PSO J030947.49+271757.31 must be relatively low–lower than about 5).

Having explored all these possibilities, we are left to scrutinize the definiteness of the claim that the radio-loud quasar population indeed declines substantially at high-*z* (Volonteri et al. 2011). To start with, it is important to note that their inferences rely on normalizing the number of sources (high-*z* blazars and luminous SDSS+FIRST quasars) by the luminosity functions of their parent populations. This normalization is particularly uncertain when it comes to the highest redshift blazars. Ajello et al. (2009) derived deconvolved all-sky values based on the number of sources that were observed with an optimal detector, which can lead to non-negligible correction factors. Second, since the Swift-BAT survey found zero blazars at $z > 4$, the quoted number of sources in the $4 - 5$ and $5 - 6$ redshift bins in Volonteri et al. (2011) are actually based on the "minimal

evolution" blazar luminosity function proposed by Ghisellini et al. (2010), rather than detections. Noting that the luminosity function derived by Ajello et al. (2009) exceeded the maximum number density of massive black holes allowed by the standard relationships between dark matter halos, galaxies, and their central black holes, Ghisellini et al. (2010) imposed an exponential cutoff to the Ajello et al. function above its peak, i.e. at $z = 4.3$ (we emphasize that the peak number density itself was poorly constrained, owing to zero blazars detected at $z > 4$ and only five at $3 < z < 4$).

While a significant population of $z > 4$ blazars has been discovered since (e.g., Ghisellini et al. 2015b; Caccianiga et al. 2019; Belladitta et al. 2020, and references therein), which may still be in tension with the small number of known $z > 4$ radio galaxies, considerable uncertainty remains in the appropriate luminosity function. The Caccianiga et al. (2019) sample is part of a complete, flux-limited sample of radio-selected blazars, for which the number density peaks at $z \simeq 2$, as opposed to $z \simeq 4$ for the Ajello et al. (2009) sample. The peak at $z \simeq 2$ is consistent with both radio-selected, radio-loud quasars (Mao et al. 2017) and radio-quiet quasars (Hopkins et al. 2007). The volume density of these blazars at $4 < z < 5$ is ≈ 0.1 Gpc^{-3} (Ighina et al. 2019), and since only the few most luminous are BAT sources, this suggests that the expected radio-loud quasar number density at the luminosity threshold adopted by Volonteri et al. (2011) is substantially lower, thus strongly reducing the tension between the number of blazars and radio-loud quasars at $z > 4$. However, it is not clear whether the discrepancy with Ajello et al. (2009) results from the radio and X-ray selection functions sampling very different objects, or if the most luminous blazars, seen with BAT and tracing the most massive black holes, evolve differently.

Meanwhile, an updated quasar bolometric luminosity function (Shen et al. 2020) revises the normalization downwards relative to Hopkins et al. (2007), and has a steeper slope at $\gtrsim 10^{46}$ erg s^{-1} and $z \gtrsim 2$. For a given radio-loud fraction, this would tend to worsen the discrepancy highlighted by Volonteri et al. (2011), but may also require a revision of the Ghisellini et al. (2010) minimal evolution luminosity function.

In addition to the uncertainty in the luminosity functions, the selection of radio-loud galaxies from the SDSS+FIRST sample carries uncertainty from the quasar selection algorithm. For example, Volonteri et al. (2011) adopted the Richards et al. (2002) SDSS color selection algorithm to identify extremely luminous ($\gtrsim 10^{47}$ erg s^{-1}), radio-loud quasars, whereas, e.g., Mao et al. (2017) used a variety of data, including optical spectra and infrared colors to identify SDSS+FIRST radio-loud quasars. As Volonteri et al. (2011) point out, incompleteness bias should cancel out when measuring the radio-loud fraction in an incomplete sample, but a bias for or against classifying quasars as radio-loud with a given method (e.g., due to a lack of infrared photometry; Bañados et al. 2015) would still impact the measurement. This issue is compounded by the small number of radio-loud quasars identified by Volonteri et al. (2011) at $z \gtrsim 4$, where the statistical uncertainty and cosmic variance could easily change the reported fractions by several percent. Indeed, Bañados et al. (2015) find no evolution in the radio-loud fraction up to $z \gtrsim 6$.

To summarize, we have failed to identify a viable explanation for why the fraction of radio-loud quasars would drop substantially above $z \gtrsim 3$. Specifically, we demonstrate that IC/CMB can quench the radio lobes of high-z jetted AGN, but up to $z \gtrsim 6$ it cannot quench the radio emission from their hot spots. On the other hand, we argue that the reported tension between the observed and expected radio-loud fraction is substantially uncertain because the luminous blazar luminosity function is uncertain at $z \gtrsim 3$, and because there is uncertainty in the classification of quasars as radio-loud or radio-quiet, with a magnitude that depends on the available data. Thus, both the expected number of radio-loud quasars based on the blazar luminosity function and the expected number extrapolated from the measured radio-loud fraction are probably known imprecisely. The true magnitude of the tension, if any, remains unclear.

6 CONCLUSIONS

We have undertaken a critical, definitive assessment of the role of IC scattering of CMB photons in the context of radio galaxies. At low-z, cooling of relativistic particles in the magnetized, jet-powered lobes and hot spots is typically dominated by radio synchrotron emission, and IC/CMB is negligible. Because of the steep, $\propto (1 + z)^4$ dependence of the CMB radiation energy density, IC/CMB is supposed to become progressively more important with respect to synchrotron cooling as the redshift increases. For typical energies at play, this process will boost CMB photons into the X-ray band, and is thus expected to yield a z-dependent, concurrent X-ray brightening and radio dimming of the extended jet-powered structures. Yet, observational evidence for this seemingly unavoidable effect so far remains sparse and controversial.

Here we show that high-resolution radio and X-ray imaging data, where the emission from the hot spots can be separated out from the lobes, are necessary to properly assess and quantify the role of IC/CMB. This is because, in addition to redshift, the expected X-ray luminosity arising from IC/CMB depends on the strength of the magnetic field. Under the assumption of equipartition, the latter can be expressed in terms of the radio luminosity and size of the emitting region (Equation 4). Accordingly, whereas IC/CMB can be expected to play a significant role in cooling the extended, weakly dominated lobes, it will be more easily offset by synchrotron and SSC cooling in the compact, highly magnetized hot spots.

Analysing spatially resolved radio and X-ray data for sample of 11 high-z radio galaxies ($1.3 \lesssim z \lesssim 4.3$) we demonstrate that:

- X-ray emission from the lobes is fully consistent with the expectations from IC/CMB in equipartition (Figure 2). This is true regardless of redshift, AGN luminosity, and lobe size (Figure 3).
- In contrast, X-ray emission from the hot spots of the high-z radio galaxies in our sample is consistent with the expectation from SSC in equipartition (Figure 4).
- The galaxy sample examined in this work is likely to be both the high-z analog of local radio galaxies, as well as a fair a representation of the broader population of high-z radio galaxies, in that they appear to be close to equipartition over a wide range in power and size. Although this sample does not include radio galaxies up to the highest redshifts to which blazars have been detected, the high-z radio galaxies in this sample are consistent with being the misaligned counterparts of the luminous blazars studied in Ghisellini et al. (2010).
- Once the dependence on size and radio luminosity are property accounted for, the measured lobe X-ray luminosity does indeed bear the characteristic $\propto (1 + z)^4$ dependence expected of a CMB seed radiation field (Figure 5).

- IC/CMB causes a concurrent, z-dependent X-ray brightening/radio dimming of the lobes of radio galaxies. Whereas this effect can quench the radio emission from the lobes of high-z radio galaxies (above $z \gtrsim 3$) below the sensitivity threshold of the FIRST survey, it would not be sufficient to quench the radio emission from their strongly magnetized hot spots at $z \lesssim 6$. Thus, IC/CMB alone can not be responsible for a deficit in high-z, radio-loud AGN if–as we argue–such AGN typically have bright hot spots.

DATA AVAILABILITY

The data used in this work are publicly available through the VLA data archive (https://science.nrao.edu/facilities/vla/archive/index) and the Chandra data archive (https://cxc.cfa.harvard.edu/cda/), using the project codes and ObsIDs from Table 1. Where necessary, the data were processed using standard tools for each telescope available from those facilities.

REFERENCES

Ajello M., et al., 2009, ApJ, 699, 603
Bañados E., et al., 2015, ApJ, 804, 118
Belladitta S., et al., 2020, A&A, 635, L7
Bennett C. L., Larson D., Weiland J. L., Hinshaw G., 2014, ApJ, 794, 135
Bîrzan L., McNamara B. R., Nulsen P. E. J., Carilli C. L., Wise M. W., 2008, ApJ, 686, 859
Caccianiga A., et al., 2019, MNRAS, 484, 204
Capetti A., Massaro F., Baldi R. D., 2017, A&A, 601, A81
Croston J. H., Hardcastle M. J., Harris D. E., Belsole E., Birkinshaw M., Worrall D. M., 2005, ApJ, 626, 733
Fabian A. C., 2012, ARA&A, 50, 455
Fanaroff B. L., Riley J. M., 1974, MNRAS, 167, 31P
Fender R. P., Belloni T. M., Gallo E., 2004, MNRAS, 355, 1105
Fruscione A., et al., 2006, in Silva D. R., Doxsey R. E., eds, Society of Photo-Optical Instrumentation Engineers (SPIE) Conference Series Vol. 6270,

Society of Photo-Optical Instrumentation Engineers (SPIE) Conference Series. p. 62701V, doi:10.1117/12.671760
Georganopoulos M., Meyer E., Perlman E., 2016, Galaxies, 4, 65
Ghisellini G., 2013, Radiative Processes in High Energy Astrophysics. Vol. 873, Springer International Publishing Switzerland, doi:10.1007/978-3-319-00612-3
Ghisellini G., et al., 2010, MNRAS, 405, 387
Ghisellini G., Celotti A., Tavecchio F., Haardt F., Sbarrato T., 2014, MNRAS, 438, 2694
Ghisellini G., Haardt F., Ciardi B., Sbarrato T., Gallo E., Tavecchio F., Celotti A., 2015a, MNRAS, 452, 3457
Ghisellini G., Haardt F., Ciardi B., Sbarrato T., Gallo E., Tavecchio F., Celotti A., 2015b, MNRAS, 452, 3457
HI4PI Collaboration et al., 2016, A&A, 594, A116
Hardcastle M. J., Harris D. E., Worrall D. M., Birkinshaw M., 2004, ApJ, 612, 729
Hardcastle M. J., Croston J. H., Kraft R. P., 2007, ApJ, 669, 893
Harwood J. J., et al., 2016, MNRAS, 458, 4443
Hopkins P. F., Richards G. T., Hernquist L., 2007, ApJ, 654, 731
Ighina L., Caccianiga A., Moretti A., Belladitta S., Della Ceca R., Ballo L., Dallacasa D., 2019, MNRAS, 489, 2732
Jiang L., Fan X., Ivezić Ž., Richards G. T., Schneider D. P., Strauss M. A., Kelly B. C., 2007, ApJ, 656, 680
Kataoka J., Stawarz Ł., 2005, ApJ, 622, 797
Kellermann K. I., Sramek R., Schmidt M., Shaffer D. B., Green R., 1989, AJ, 98, 1195
Mao P., Urry C. M., Marchesini E., Land oni M., Massaro F., Ajello M., 2017, ApJ, 842, 87
McMullin J. P., Waters B., Schiebel D., Young W., Golap K., 2007, in Shaw R. A., Hill F., Bell D. J., eds, Astronomical Society of the Pacific Conference Series Vol. 376, Astronomical Data Analysis Software and Systems XVI. p. 127
Meyer E. T., Georganopoulos M., Sparks W. B., Godfrey L., Lovell J. E. J., Perlman E., 2015, ApJ, 805, 154
Miller B. P., Brandt W. N., Schneider D. P., Gibson R. R., Steffen A. T., Wu J., 2011, ApJ, 726, 20
Moster B. P., Somerville R. S., Maulbetsch C., van den Bosch F. C., Macciò A. V., Naab T., Oser L., 2010, ApJ, 710, 903
Nagar N. M., Falcke H., Wilson A. S., 2005, A&A, 435, 521
Napier K., Foord A., Gallo E., Ghisellini G., Hodges-Kluck E., Wu J., Haardt F., Ciardi B., 2020, MNRAS, 498, 1550
O'Dea C. P., 1998, PASP, 110, 493
Pacholczyk A. G., 1970, Radio astrophysics. Nonthermal processes in galactic and extragalactic sources. Freeman
Padovani P., 1993, MNRAS, 263, 461
Reines A. E., Condon J. J., Darling J., Greene J. E., 2020, ApJ, 888, 36
Richards G. T., et al., 2002, AJ, 123, 2945
Schwartz D., et al., 2020, arXiv e-prints, p. arXiv:2010.06535
Shen Y., et al., 2011, ApJS, 194, 45
Shen X., Hopkins P. F., Faucher-Giguère C.-A., Alexander D. M., Richards G. T., Ross N. P., Hickox R. C., 2020, MNRAS, 495, 3252
Simionescu A., et al., 2016, ApJ, 816, L15
Smail I., Blundell K. M., 2013, MNRAS, 434, 3246
Smail I., Blundell K. M., Lehmer B. D., Alexand er D. M., 2012, ApJ, 760, 132
Spingola C., Dallacasa D., Belladitta S., Caccianiga A., Giroletti M., Moretti A., Orienti M., 2020, A&A, 643, L12
Tadhunter C., et al., 2011, MNRAS, 412, 960
Vasudevan R. V., Fabian A. C., 2007, MNRAS, 381, 1235
Volonteri M., Haardt F., Ghisellini G., Della Ceca R., 2011, MNRAS, 416, 216
Worrall D. M., 2009, A&A Rev., 17, 1
Worrall D. M., Birkinshaw M., 2006, Multiwavelength Evidence of the Physical Processes in Radio Jets. Springer, Berlin and Heidelberg, p. 39, doi:10.1007/3-540-34621-X_2

Worrall D. M., Birkinshaw M., Marshall H. L., Schwartz D. A., Siemigi-nowska A., Wardle J. F. C., 2020, MNRAS, 497, 988

Wu J., Brandt W. N., Miller B. P., Garmire G. P., Schneider D. P., Vignali C., 2013, ApJ, 763, 109

Wu J., Ghisellini G., Hodges-Kluck E., Gallo E., Ciardi B., Haardt F., Sbarrato T., Tavecchio F., 2017, MNRAS, 468, 109

Zhu S. F., Brandt W. N., Wu J., Garmire G. P., Miller B. P., 2019, MNRAS, 482, 2016